Journal of Hydrology 602 (2021) 126771

Contents lists available at ScienceDirect

Journal of Hydrology

journal homepage: www.elsevier.com/locate/jhydrol

Research papers

Simulating site-scale permafrost hydrology: Sensitivity to modelling decisions and air temperature

Sebastian A. Krogh [a,b,*], John W. Pomeroy [a]

[a] Centre for Hydrology, University of Saskatchewan, 1151 Sidney Street, Canmore, Alberta T1W 3G1, Canada
[b] Departamento de Recursos Hídricos, Facultad de Ingeniería Agrícola, Universidad de Concepción, Avda. Vicente Méndez 595, Chillán, Ñuble 3812120, Chile

ARTICLE INFO

This manuscript was handled by Marco Borga, Editor-in-Chief, with the assistance of Francesco Avanzi, Associate Editor

Keywords:
Permafrost hydrology
Arctic
Cold regions
Hydrological modelling
Model uncertainty

ABSTRACT

To predict future hydrological cycling in permafrost-dominated regions requires consideration of complex hydrological interactions that involve cryospheric states and fluxes, and hence thermodynamics. This challenges many hydrological models, particularly those applied in the Arctic. This study presents the implementation and validation of set of algorithms representing permafrost and frozen ground dynamics, coupled into a physically based, modular, cold regions hydrological model at two tundra sites in northern Yukon Territory, Canada. Hydrological processes represented in the model include evapotranspiration, soil moisture dynamics, flow through organic and mineral terrain, ground freeze–thaw, infiltration to frozen and unfrozen soils, snowpack energy balance, and the accumulation, wind redistribution, sublimation, and canopy interception of snow. The model was able to successfully represent observed ground surface temperature, ground thaw and snow accumulation at the two sites without calibration. A sensitivity analysis of simulated ground thaw revealed that the soil properties of the upper organic layer dominated the model response; however, its performance was robust for a range of realistic physical parameters. Different modelling decisions were assessed by removing the physically based algorithms for snowpack dynamics and ground surface temperature and replacing them with empirical approaches. Results demonstrate that more physically based approaches should be pursued to reduce uncertainties in poorly monitored environments. Finally, the model was driven by three climate warming scenarios to assess the sensitivity of snow redistribution and ablation processes and ground thaw to warming temperatures. This showed great sensitivity of snow regime and soil thaw to warming, even in the cold continental climate of the northwestern Canadian Arctic. The results are pertinent to transportation infrastructure and water management in this remote, cold, sparsely gauged region where traditional approaches to hydrological prediction are not possible.

1. Introduction

The warming Arctic is undergoing several environmental changes such as shrub expansion and densification (Lantz et al., 2013; Myers-Smith et al., 2018; Sturm et al., 2001), permafrost thaw (Payette, 2004) and declines in terrestrial water storage (Suzuki et al., 2018). Permafrost thaw has been shown to be critical for hydrological connectivity, supra- and super-permafrost groundwater exchange, hydraulic conductivity and subsurface runoff and storage (Walvoord and Kurylyk, 2016), carbon dioxide and methane release (Herndon, 2018; Knoblauch et al., 2018), changes in landscape (Liljedahl et al., 2016; Myers-Smith et al., 2008) and infrastructure such as building foundations and roadbed stability. Therefore, a better understanding of and ability to predict permafrost thaw and its hydrological consequences are needed in the context of climate and vegetation change.

Simulating the ground freeze and thaw regime represents a great challenge as it is the result of complex interactions between processes representing the energy and mass exchanges amongst atmosphere, land, snowpack and subsurface (Kane et al., 1991; Park et al., 2015; Woo, 2012; Yamazaki, 2001; Zhao et al., 1997). Numerical methods representing the heat transfer equation, including heat conduction, latent heat and convective heat exchange, coupled with subsurface flow have been shown to properly simulate ground freeze and thaw, using detailed ground information and forcing data (Kurylyk and Watanabe, 2013). Models like the Advance Terrestrial Simulator (ATS; Atchley et al., 2015; Jan et al., 2020; Jan et al., 2018; Painter et al., 2016), SUTRA-ICE

* Corresponding author.
E-mail address: skrogh@udec.cl (S.A. Krogh).

https://doi.org/10.1016/j.jhydrol.2021.126771
Received 11 April 2021; Received in revised form 14 July 2021; Accepted 28 July 2021
Available online 2 August 2021

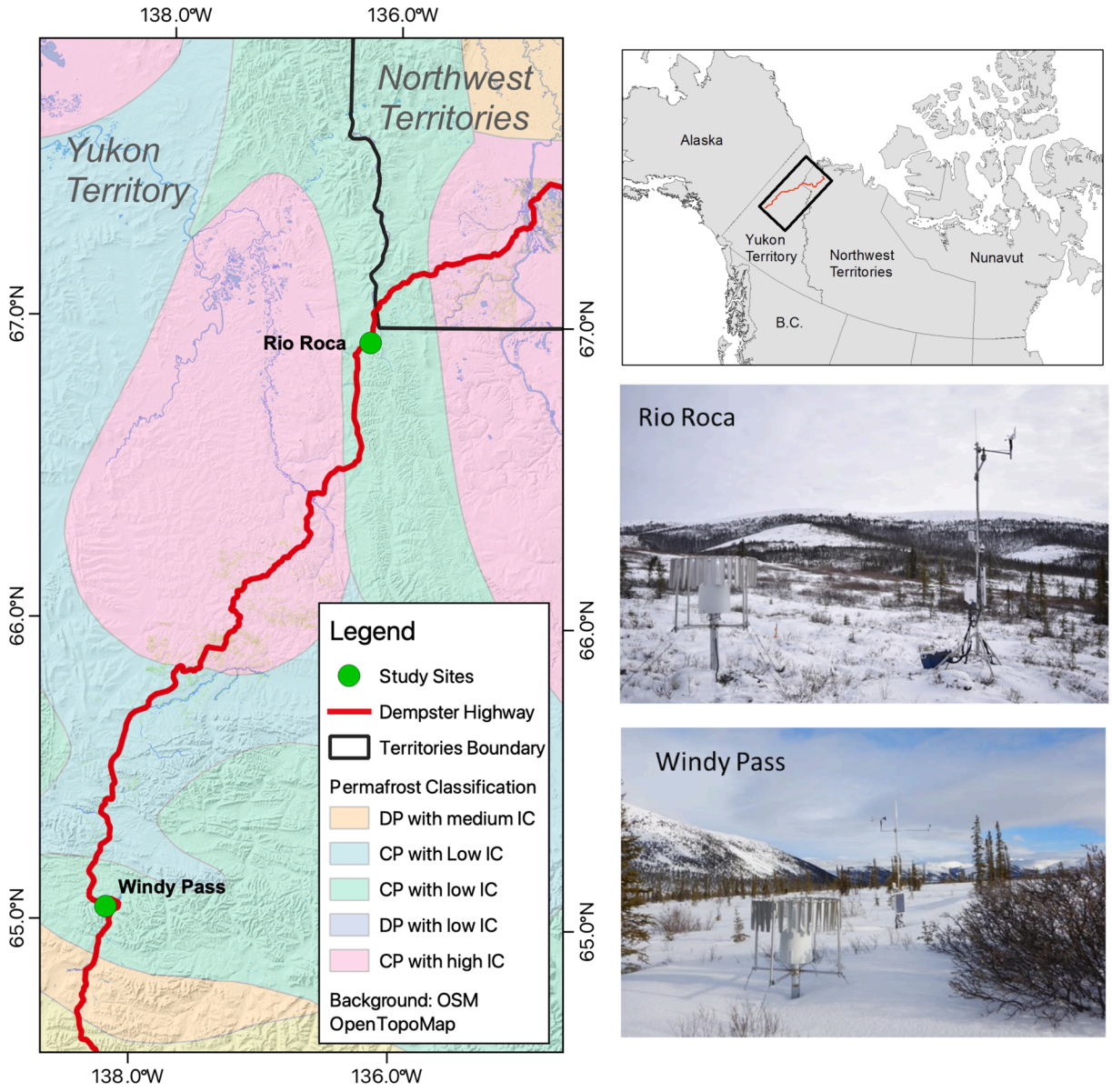

Fig. 1. Location of permafrost hydrology study sites in northern Yukon Territory, Canada. Permafrost classification and delineation from Brown et al. (2002), where CP and DP refer to Continuous and Discontinuous Permafrost, respectively, and IC is Ice Content. Low IC is below 10%, medium IC is between 10% and 20% and high IC is above 20%.

(McKenzie et al., 2007) and GEOtop (Endrizzi et al., 2014) have been extensively tested, demonstrating their ability to represent the hydrological and thermal regime of the Arctic. However, their main disadvantage is that they are data-intensive and computationally expensive, which may preclude their implementation in regions of the Arctic that are not heavily monitored or when needed to be applied at large scales for hydrological applications. Conversely, there are simplified, empirical representations for the active layer thickness based on empirical equations (e.g. degree-day), which have been used for hydrological modelling in cold regions (Kane et al., 1997; Schramm et al., 2007; Zhang et al., 2000). The main disadvantage of these approaches is that they are not reliable under conditions different from which they were developed (Sivapalan, 2003), limiting their implementation in remote and ungauged or poorly-gauged regions, and for climate change impact studies, for which more physically based approaches should be pursued instead (Pomeroy et al., 2013). Therefore, models of more intermediate complexities that can reliably represent ground freeze and thaw, among other critical Arctic and subarctic processes, and can be relatively easily implemented in hydrological models are needed to allow multiple model realizations and assess model uncertainty and sensitivity.

In the context of models of intermediate complexity, Stefan's Equation (Juminikis 1977, p. 205) is a commonly used and relatively simple one-directional model that estimates ground freeze and thaw in homogeneous soils, which considers the latent heat of fusion and neglects the soil volumetric heat capacity and convective heat exchange. Modified versions of Stefan's Equation have been developed to be implemented in multilayered soils (Fox, 1992; Hayashi et al., 2007; Woo et al., 2004; Yi et al., 2006). Another modified version of Stefan's Equation developed by Xie and Gough (2013), referred as the XG-algorithm, differs from previous approaches as it does not require averaging of soil parameters for multilayered soils and is independent of the number and thickness of soil layers. Algorithms based on Stefan's Equation require ground surface temperature estimation as the upper boundary condition. Measuring this variable is not common and even if it is measured at a point, spatially distributed estimations are required for hydrological models. Simulation of ground surface temperature has been typically

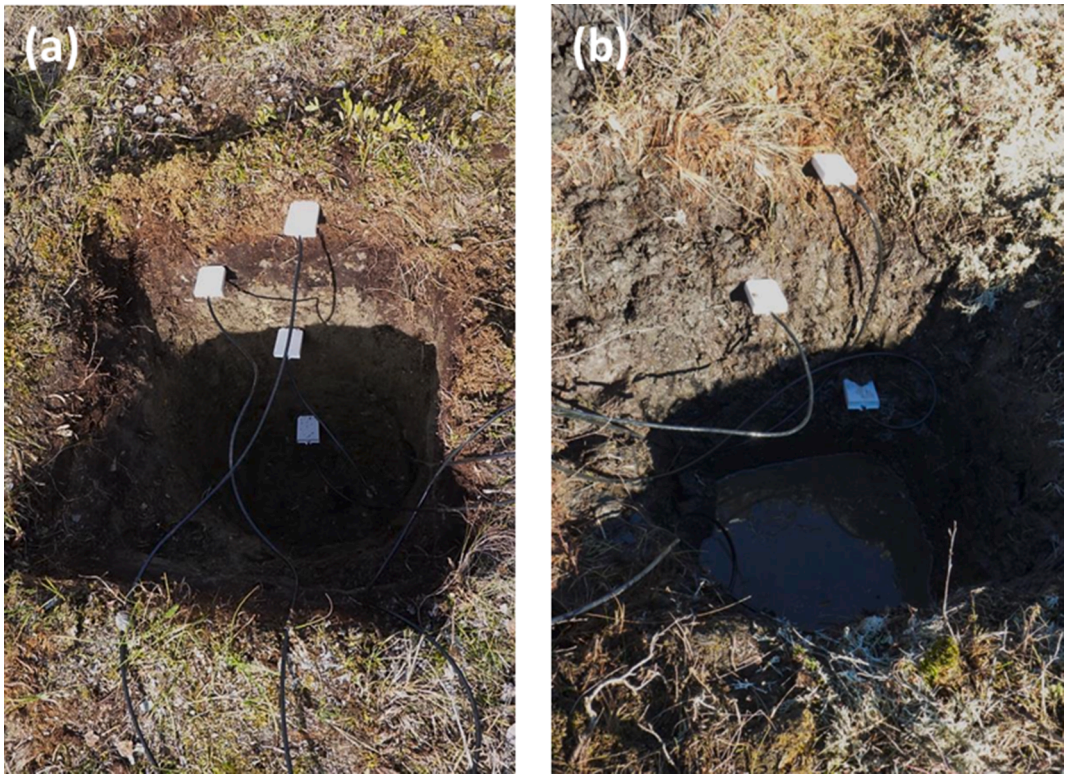

Fig. 2. (a) Soil profile at Windy Pass, September 6, 2014, where permafrost was not reached. (b) Soil profile at Rio Roca, September 7, 2014, where ice-rich permafrost was reached and limited further digging.

Table 1
Instrumentation at the two research sites.

Measurement	Manufacturer	Model	Quantity	Sensor height or depth (m) with respect to ground surface	
				Windy Pass	Rio Roca
Precipitation	Ott	Pluvio2	1	2.0	2.0
Air Temperature and Relative Humidity	Rotronic	HC-S3-XT	1	2.1	2.9
Outgoing and Incoming Shortwave Radiation	Apogee	SP-230	1 (each)	2.0 and 2.4, respectively	4.1 and 4.3, respectively
Wind Speed and Direction	RM Young	05108-10-L	1	4.3	5.0
Snow Depth	Campbell	CSI SR50A	1	2.2	2.5
Soil Heat Flux	Hukseflux	HFP01-L	1	−0.03	−0.03
Soil Moisture and Temperature	Campbell	CS655-L	4	−0.1, −0.23, −0.51, −0.91	−0.1, −0.3, −0.5, −0.76
Ground Surface Temperature	Omega	Type E Thermocouple	1	−0.01	−0.01

approached by implementing a ratio between ground surface temperature to air temperature, referred as the n-factor (Woo 2012, p. 56), which is commonly assumed to be constant. Main issues associated to the use of the n-factor are its empirical basis and that it varies spatially (Klene et al., 2001) and temporally (Woo et al., 2007). Williams et al. (2015) presented a novel approach to estimate ground surface temperature based on air temperature, net radiation, and ground thaw depth, referred as the Radiative-Conductive-Convective (RCC) approach. The RCC approach showed good performance at three research basins in northern Canada, and it proved to have a superior performance over the empirical n-factor. Both the XG-algorithm and the RCC approach were incorporated in the Cold Regions Hydrological Modelling Platform (CRHM; Pomeroy et al. 2007), and they are part of the Arctic Hydrology Model (AHM) developed by Krogh et al. (2017) using CRHM and applied by Krogh and Pomeroy (2019); Krogh and Pomeroy (2018) to investigate historical and future hydrological changes in an Arctic basin under transient climate and vegetation.

This study investigates the incorporation of the XG-algorithm and RCC approach into the CRHM-AHM using detailed ground observations and demonstrates why more physically based models of intermediate complexity should be pursued instead of empirical approaches, particularly in cold, remote and poorly monitored regions. As a secondary goal, the sensitivity of the model to changes in the soil thermal properties and porosity is also examined for model transferability and climate change studies. Finally, three warming air temperature scenarios are assessed to investigate the vulnerability of this region to projected changes in air temperature. To pursue these goals, the model is applied at a site-scale to two well-instrumented tundra research sites in northern Yukon Territory, Canada, for which measurements of soil temperature, ground surface temperature, snowpack and meteorological variables are available.

2. Study sites and data

The two sites selected for this study in northern Yukon Territory, Canada (Fig. 1) are Rio Roca (66° 50′ 1.0′’ N, 136° 20′ 0.0′’ W) and

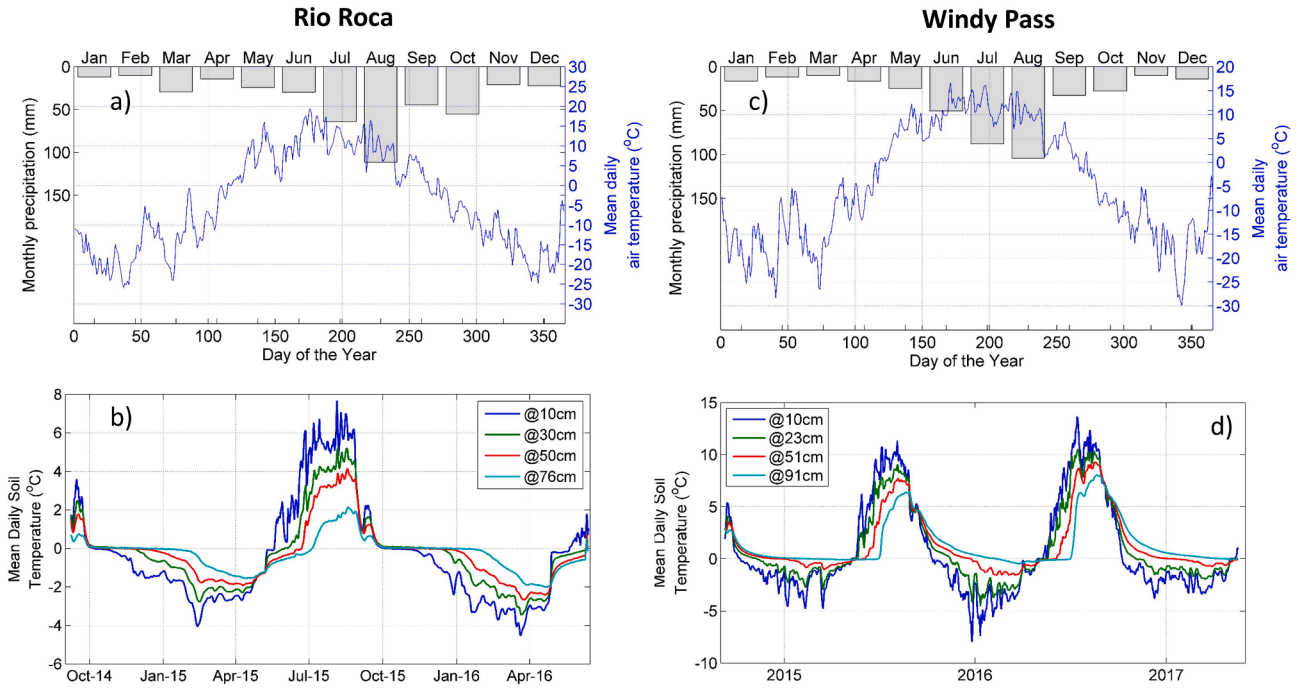

Fig. 3. Mean observed records for monthly precipitation (corrected by wind undercatch) and daily air temperature at Rio Roca (a) and Windy Pass (b), and ground temperature at four different depths for Rio Roca (c) and Windy Pass (d).

Windy Pass (65° 4′ 0.8′′ N, 138° 14′ 46.1′′ W). These sites were selected as they represent the sparsely wooded tundra drainage basins of the region, have good access from the only road in northern Yukon, the Dempster Highway, are relatively sheltered from wind and bridge the gap between existing weather stations along the Dempster Highway corridor. The elevation at Windy Pass is 1,030 m.a.s.L. in a terrain with a mild slope estimated at 5° and surrounded by shrubs, moss, and scattered spruce. The soil profile at Windy Pass is characterized by an upper partially decomposed organic layer (23 cm thick), followed by a denser organic matter layer (15 cm thick), underlain by mineral soil (Fig. 2a). The elevation at Rio Roca is 660 m.a.s.L., with a ground surface slope estimated at 4°, is surrounded by scattered shrubs and spruce, and with moss, lichen, and grass on the ground. The soil profile at Rio Roca is characterized by an upper partially decomposed organic layer (18 cm thick), followed by a denser and organic matter layer of at least 63 cm thickness, at which point, continuous, ice-rich permafrost was reached, and further subsoil investigations were not possible (Fig. 2b). According to the Brown et al. (2002) permafrost classification shown in Fig. 1, both sites are underlain by continuous permafrost with low ice content (<10%); however, we found that that was not case for the Rio Roca site (Fig. 2b).

Both stations were equipped with sensors to measure the following variables: precipitation, air temperature, relative humidity, incoming and outgoing shortwave radiation, wind direction and speed, snow depth, soil heat flux, soil moisture and temperature (four depths), ground surface temperature and snow temperature. The sensors' models, manufacturers and height/depths are detailed in Table 1. The data was recorded using a CR1000 datalogger from Campbell Scientific Canada Ltd., and the frequency of measurements was every 30 min for all variables except for soil moisture and temperature, which were measured every 6 h.

2.1. Observed hydrometeorological conditions

2.1.1. Rio Roca

Continuous records are available from September 2014 until June 2016, when this site was damaged by a bear; therefore, only one ground thaw season (2015) and two winter seasons (2014–2015 and 2015–2016) are available. Fig. 3a presents mean monthly precipitation and mean daily temperature for the observed period. Precipitation was corrected for the effect of wind undercatch, typically found for snowfall in cold, windy and dry environments (Goodison et al., 1998), using the empirical relationship between wind speed and undercatch developed by Smith (2008). Mean annual precipitation was 439 mm, for which the maximum monthly precipitation occurred in August at 111 mm. Mean summer precipitation (June to August) was 205 mm or 47% of the mean annual precipitation, whereas winter precipitation (October to April) accounted for 165 mm or 38% of the mean annual precipitation. Mean annual air temperature at Rio Roca was −4.1 °C, and the maximum and minimum recorded temperatures were 25.5 and −36.3 °C, respectively, with an average > 0 °C season of 150 days, from April 25 to September 22. Wind speed was relatively mild, with most events below 4 m s^{-1}; however, some isolated event reached up top 10 m s^{-1}. Fig. 3b presents mean daily soil temperature at four depths, showing the duration of ground thawing and freezing seasons (Table A1). Note that ground temperature at all depths go well below 0 °C, supporting the presence of continuous permafrost as shown by the Brown et al. (2002) classification shown in Fig. 1.

2.1.2. Windy Pass

Continuous weather and soil data is available from September 2014 to June 2017, including two summers (2015 and 2016) and three winters (2014–2015, 2015–2016 and 2016–2017). Fig. 3c presents mean monthly precipitation and mean daily air temperature. Precipitation was also corrected for the effect of wind undercatch using the expression from Smith (2008). Corrected mean annual precipitation was 407 mm (slightly drier than Rio Roca), with a maximum in August at 104 mm, and a total summer precipitation of 243 mm or 60% of the mean annual precipitation. Winter precipitation (October to April) was 107 mm or 26% of the mean annual precipitation. Mean annual temperature was −4.4 °C (colder than Rio Roca), and the maximum and minimum recorded temperatures were 25.0 and −42.1 °C respectively, with an

average > 0 °C season of 148 days from April 28 to September 23. Winds were relatively mild, and typically below 2 m s^{-1}, but reached up to 8 m s^{-1}. Fig. 3d presents mean daily soil temperature at four depths, showing the duration of the thawing season, which was shorter in 2015 than in 2016. Table A2 presents a summary with the initiation, duration and end of ground thawing and freezing for the two water years. In general, the deeper into the ground the longer the thawing season is at Windy Pass, which is the opposite of the colder Rio Roca site.

3. Hydrological model: site-scale application

The Arctic Hydrology Model (AHM; Krogh et al., 2017), developed using the Cold Regions Hydrological Model platform (CRHM; Pomeroy et al., 2007; Pomeroy et al., 2016), was used to simulate surface and subsurface mass and energy interactions at Windy Pass and Rio Roca. The CRHM-AHM model is a physically-based and semi-distributed hydrological model that uses hydrological response units to compute the energy and mass balance. When run at a site-scale, as in this application, the model is composed of a single hydrological response unit that represent the scale of the site where hydrological and atmospheric observations are taken, and thus, it lacks a streamflow routing routine. Hydrological processes represented in this application include snow albedo decay, precipitation phase, sublimation/evaporation from canopy, intercepted snowfall/rainfall, snowpack mass and energy balance, snow redistribution and sublimation by wind, ground freeze and thaw, evaporation and transpiration, surface and subsurface flow and storage, runoff (detention flow) through organic terrain and snowpack, and infiltration into frozen and unfrozen soils. A brief description with the key characteristics of each module representing the hydrological processes are presented in Table A3; however, a more detailed description can be found in Krogh et al. (2017) for a basin-scale application. Most algorithms used to represent these hydrological processes have a strong physical basis, allowing confidence in the model and parameter transferability between sites with similar conditions. The CRHM-AHM requires hourly input forcing data consisting of precipitation, air temperature, relative humidity, wind speed and shortwave irradiance. Longwave irradiance was estimated in the model using the method presented by Sicart et al. (2006).

As a fine-scale implementation of the CRHM-AHM model to fairly flat sites, this application did not allow horizontal inputs of liquid water fluxes such as surface and subsurface flow, though water can flow out and blowing snow can also be transferred horizontally through wind redistribution. The majority of the parameters used in this study are presented and discussed by Krogh et al. (2017), which were taken from detailed process studies in the region or in places with similar hydrological conditions; however, parameters describing local characteristics such as elevation, aspect, slope, vegetation and soil profile are specific to each site and derived from local measurements. The interactions between subsurface physical processes within CRHM-AHM are shown in the Fig. 4 of Krogh et al. (2017), which is the same model structure as used here.

To simulate the seasonal thawing and freezing of the ground the CRHM-AHM model uses the XG-algorithm (Xie and Gough, 2013), which is a simplified solution for Stefan's equation that allows multi-layered soil with non-uniform soil properties. This method only considers the latent heat of fusion and neglects the volumetric heat capacity of the soil associated with sensible heat fluxes and heat advection, and thus, it assumes a uniform temperature profile at the freezing point (0 °C) below the thawing front. The XG-algorithm simulates a freezing/thawing front from the ground surface downward based on a surface freeze/thaw index (degree-day) and assumes a linear temperature profile within soil layers. As such, it requires estimates of ground surface temperature to provide the upper boundary condition to the model. The ground surface temperature is estimated using the RCC approach (Williams et al., 2015). The soil profile configuration used here consists of 20 soil layers, which represent the upper-most three meters of the ground. Records of soil temperature show that below 1.5 m the soil does not thaw, and thus, a three-meter ground layer is sufficient to represent the seasonal freezing and thawing of the active layer.

The top 10 layers are 0.1 m thick and the lower 10 layers are 0.2 m thick. The top 4 layers in the Windy Pass model represent the top organic soil and the lower 16 layers represent the mineral soil (Fig. 2a). The Rio Roca model has a thicker organic layer represented by the top 8 layers in the model and the mineral soil represented by the remaining 12 layers (Fig. 2b). The thermal properties and porosities used in the organic and mineral soil layers are based on reference values presented by Woo (2012). For the organic soil layer the porosity, dry thermal conductivity, saturated unfrozen thermal conductivity, saturated frozen thermal conductivity was set to 0.8, 0.1 W m^{-1} K^{-1}, 1.0 W m^{-1} K^{-1} and 1.9 W m^{-1} K^{-1}, respectively. Whereas the same parameters for the mineral soil layer were set to 0.4, 0.25 W m^{-1} K^{-1}, 2.5 W m^{-1} K^{-1} and 1.9 W m^{-1} K^{-1}, respectively. The CRHM-AHM model uses the relationships from Johansen (1975, p. 221) to calculate the thermal conductivity of non-saturated soils based on the degree of saturation of the soil and saturated thermal conductivity.

3.1. Parameter sensitivity analysis

To quantify the uncertainty on simulated ground thaw associated with the typically most uncertain subsurface parameter, a sensitivity analysis for a range of possible and documented values was performed. The six parameters included in the sensitivity analysis and their range were the dry thermal conductivity (ranging between [0.06–0.15] and [0.2–0.3] W m^{-1} K^{-1} for the organic and soil layers, respectively), unfrozen saturated thermal conductivity (ranging between [0.25–0.75] and [2.0–3.0] W m^{-1} K^{-1} for organic and soil layers, respectively), and porosity (ranging between [0.7–0.9] and [0.3–0.5] for organic and soil layers, respectively).

We used the global sensitivity analysis developed by Razavi and Gupta (2016), referred as VARS (Variogram Analysis of Response Surfaces), in particular the "STAR-VAR" implementation was used. This method accounts for the spatial ordered structure of the model response across the parameter range, which is typically neglected in other methods (Razavi et al., 2019). This implementation requires a number of "STARS" to determine how many model iterations to be performed. Here, 15 STARS and a "resolution" of sampling h = 0.1 (recommended value by Razavi et al., 2019)) were used, resulting in 825 model iterations. To quantify the global sensitivity of the model we used the Integrated Variogram Analysis between the 0 and 50% of the parameter range, typically referred as $IVARS_{50}$. The objective function to measure the sensitivity of the model is based on the mean bias between observed and simulated ground thaw at four depths.

3.2. Modelling decision analysis

A model experiment was run using model configurations with different levels of complexities to evaluate the importance of pursuing more physically based approaches to represent key physical processes in Arctic environments. This took advantage of CRHM's flexible modular structure to swap and replace physically based modules with empirical ones, whilst leaving the rest of the model unchanged. Here, the CRHM-AHM was modified by switching the representation of snow accumulation, sublimation and melt, and ground surface temperature, as described below:

Model Configuration 1 (MC1): As opposed to using the two-layer mass and energy balance model SNOBAL (Marks et al., 1998) normally used in CRHM, which includes a calculation of sublimation losses as well as snowpack energetics, a conventional degree-day melt model was used, in which snowmelt is simulated as an empirical relationship with air temperature that is represented by a degree-day coefficient. Typically, this coefficient needs to be calibrated; however, here it is assumed that no local calibration data is available, which is a reasonable assumption

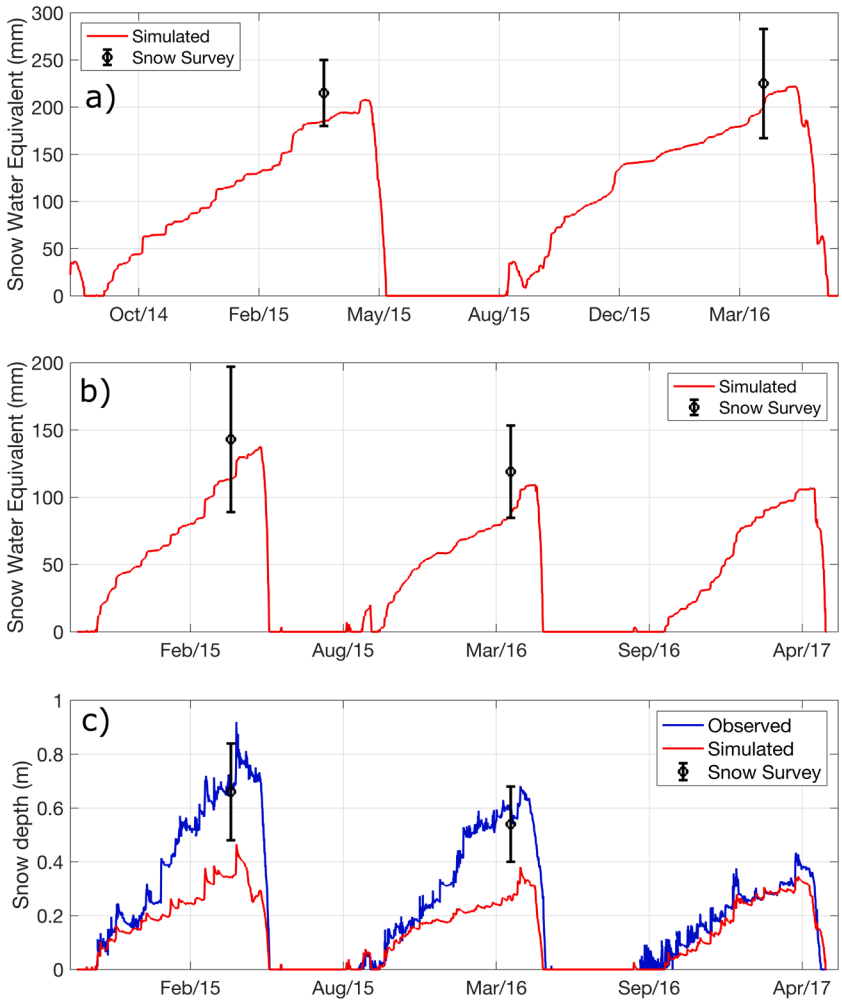

Fig. 4. Snow water equivalent validation at Rio Roca (a) and Windy Pass (b), showing the mean and standard deviation from snow survey transects. Snow depth comparison between simulations and ultrasonic snow depth sensor and a snow survey at Windy Pass (c).

in most Arctic and subarctic regions. The most reasonable estimation for the degree-day coefficient for northwestern North America is from Kane et al. (1997), who calibrated this coefficient for an Arctic basin in adjacent northern Alaska over a six-year period. The degree-day coefficient from Kane et al. (1997) that produced the best fit over the six-year period was 2.7 (mm d^{-1} $°C^{-1}$), which is the value that is used here. No attempt was made to improve the performance of this model by, for example, including a radiation component through more empirical coefficients, such as the one presented by Kustas et al. (1994), to minimize the sources of uncertainties in the experiment.

Model Configuration 2 (MC2): The algorithm normally used in CRHM to estimate ground surface temperature was changed. The RCC approach (Williams et al., 2015) was replaced with a temperature index approach (n-factor), in which ground surface temperature was calculated as a relationship with air temperature. The temperature index was the empirical relationship presented by Woo et al. (2007), which was developed using >30 years of observed data in northwestern Canada. This relationship requires three empirical coefficients: b, c and s, as well as the depth of ground thaw, as follows:

$$\frac{T_g}{T_a} = b - c*\exp(s*P) \quad (1)$$

Where T_g and T_a are the ground surface and air temperature (°C), respectively, and P is the depth of ground thaw (m). The values presented by Woo et al. (2007) for the Louisy Point, a tundra site with organic terrain in the Mackenzie Delta of the adjacent Northwest Territories, were used due to their similarly with the conditions found at Rio Roca and Windy Pass. Their values are b = 0.5, c = 0.54 and s = −0.05.

Model Configuration 3 (MC3): In this experiment, MC1 and MC2 were combined, meaning that the degree-day model was used to calculate snowmelt and the n-factor was used for the ground surface temperature.

3.3. Air temperature sensitivity

The last analysis investigates the effect of climate warming on snow accumulation and melt, and ground thaw. These variables are key in cold regions environments, controlling subsurface flow rates, runoff volume and energy exchange with the atmosphere. Three warming scenarios that increase the mean annual air temperature by 2, 4 and 6 °C were implemented, representing scenarios of moderate, significant, and severe climate warming. These scenarios can be implemented using a climate change feature of CRHM that holds relative humidity constant but allows vapour pressure to vary.

4. Results

4.1. Model validation

4.1.1. Snow water equivalent

Fig. 4 presents a comparison between simulated Snow Water

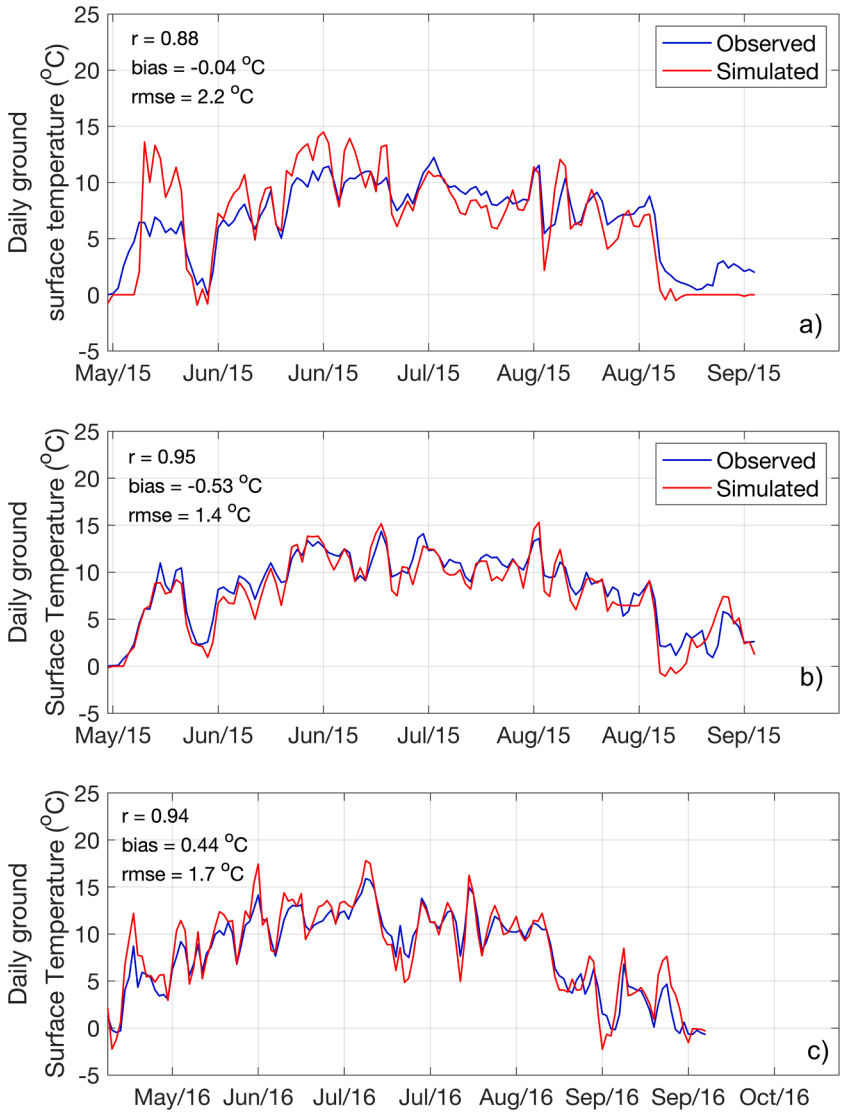

Fig. 5. Ground surface temperature comparison between observed (1 cm depth) and model. a) is for 2015 at Rio Roca and b) and c) are for 2015 and 2016 at Windy Pass.

Equivalent (SWE) against two snow surveys for water years 2014 and 2015 at the Rio Roca and Windy Pass site (Fig. 4a and 4b, respectively). Both snow surveys were performed in late March, during the accumulation season and about a month before the date of peak SWE (early May). The snow survey consisted of an approximately 25 m transect across each study site, where SWE samples were taken every 5 m. Mean and standard deviations of SWE are presented to show the degree of variability that can be found. Similar performance was found at both sites, the mean biases for the Rio Roca site were 30 and 24 mm for the water years 2014 and 2015, respectively, whereas at the Windy Pass site biases were 29 and 30 mm, respectively. Despite the underestimation at both sites, simulated SWE was within the observed SWE standard deviation. Observed SWE standard deviations suggests a relatively large spatial variability along the snow transect (both sites), due to small topographic and vegetation variations producing wind redistribution and trapping variations at scales smaller than can be modelled by the blowing snow algorithm in CRHM. Overall, the model simulations underestimated observed SWE, which may be due to uncertainty in the wind undercatch correction used (Smith, 2008), model error (e.g. calculation of blowing snow or turbulent fluxes) or biophysical and wind exposure differences between the instrument site and the snow survey transect. Continuous snow depth observations by the ultrasonic depth sensor at Windy Pass, allows evaluation of the timing of the end of snow ablation (Fig. 4c). The observed dates for the end of snow ablation for the years 2015, 2016 and 2017 were May 19, May 14 and May 9, respectively, whereas simulations were May 19, May 11 and May 15. This shows that the model simulated a 3-day earlier and 6-days later end of snow ablation period for the years 2016 and 2017, respectively, but captured the exact day in 2015. This is particularly important, as the end of the snow ablation triggers the initiation of ground thaw. Unfortunately for the Rio Roca site, records from the ultrasonic sensor were particularly noisy, precluding an accurate identification of the end of snow ablation date.

4.1.2. *Ground thaw and ground surface temperature*

Fig. 5 presents a comparison between observed ground surface daily temperature at 1 cm depth and simulations for the snow-free period of 2015 and 2016 for Windy Pass (Fig. 5a and b), and 2015 for Rio Roca (Fig. 5c). The model represents ground surface temperature well at both sites, with a slightly better performance at Windy Pass. Mean bias ranges from −0.5 and 0.4 °C at Windy Pass and −0.04 °C at Rio Roca, correlation coefficient ranges from 0.95 at Windy Pass to 0.88 at Rio Roca,

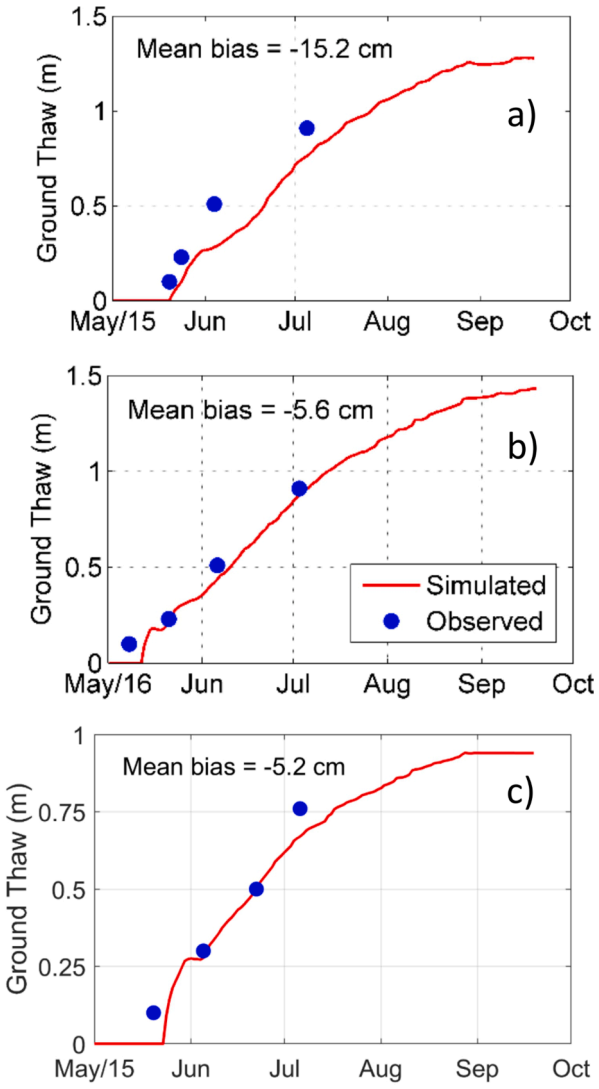

Fig. 6. Ground thaw validation at Windy Pass for the years 2015 and 2016 (a and b, respectively) and Rio Roca for the year 2015 (c).

and the root mean square error ranges from 1.4 °C at Windy Pass to 2.2 °C at Rio Roca. A slightly later (one week) initiation of ground surface thaw was simulated at Rio Roca. Overall, this analysis demonstrates the capability of the non-calibrated RCC model (Williams et al., 2015) to simulate daily ground surface temperature at Rio Roca and Windy Pass.

Fig. 6 shows simulated versus observed ground thaw for the years 2015 and 2016 at Windy Pass and 2015 at Rio Roca. Observed ground thaw was calculated by identifying the date and depth at which the soil temperature reached 0 °C, using the four soil temperature sensors. At Windy Pass, and during the thawing season of 2015, the model underestimated ground thaw by 10, 13, 23 and 15 cm at 10, 23, 51 and 91 cm deep, respectively, resulting in a mean bias of −15 cm. During the 2016 thawing season, the model also underestimated observations by 10, 2, 7 and 3 cm at 10, 23, 51 and 91 cm deep, respectively, resulting in a mean bias of −6 cm. At Rio Roca, a better agreement was found with differences of −10, 0.02, 0.0 and −9 cm, at 10, 30, 51 and 76 cm depths, respectively, resulting in a mean bias of −5 cm. The initiation of ground thaw was 5 days late and likely due to late snow ablation in the model. Overall, the model slightly underestimated ground thaw by 15 and 5 cm, which is sometimes explained by a later than observer initiation of thawing season, but also likely due to model errors; however, this is an overall good model performance considering the lack of calibration to represent ground thaw.

4.2. Ground thaw sensitivity to soil parameters

Fig. 7 presents the results of sensitivity analyses for the Rio Roca and Windy Pass models. Upper panels show the ratio of factor sensitivity using the $IVARS_{50}$ metric, as recommended by Razavi and Gupta (2016). In both cases, the parameter that had the greatest impact on the model (i.e. the largest ratio of factor sensitivity, Fig. 7a and d) was the dry thermal conductivity of the organic soil layer (p3), followed by the porosity of the organic layer (p1). Uncertainties in simulating ground thaw at both sites was estimated using the same 825 parameter-scenarios generated with VARS. At Rio Roca (Fig. 7b), little uncertainty associated with the soil parameters was found, with an active layer thickness (ALT) that varied between 0.93 and 1 m. At Windy Pass (Fig. 7e), ALT varied between 1.17 and 1.42 m for the year 2015 and between 1.31 and 1.58 m for the year 2016, revealing that the simulated ALT at Windy Pass is more sensitive to the selection of parameters, particularly those associated with the upper organic soil layer. This can be explained by the warmer and longer thawing season found at Windy Pass (Fig. 6), allowing a larger variability by the end of the season. Histograms of simulations mean bias show that at Windy Pass (Fig. 7f), parameter uncertainty alone does not completely explain the model underestimation of ground thaw, as for all the scenarios, the mean bias was always at least −6 cm. At Rio Roca (Fig. 7c), some simulations showed a mean bias of −3 cm, suggesting that with a different combination of realistic parameters the model bias can be further reduced to smaller values.

4.3. Impact of modelling decisions

Fig. 8 shows simulated SWE and ground thaw at the Rio Roca and Windy Pass site for the three model configuration experiments, and the control run, which is the model configuration using the most physically based approaches (i.e. the CRHM-AHM). SWE analysis shows a significant deterioration of simulations of snow accumulation for all years and sites under the MC1 and MC3 (i.e. degree-day for snowmelt), increasing substantially the error in simulating observed SWE. The model performance deterioration is particularly evident at the Windy Pass site, were not only observed SWE is largely underestimated, but also snow seems to be completely depleted in the middle of the 2015–2016 winter, which is highly unlike in such a cold environment, demonstrating the strong need for calibration for the empirical snow model. SWE in the MC2 shows the same performance as the control run, which is expected as the n-factor for calculating ground surface temperature does not play a role in representing snow accumulation and melt.

Ground thaw simulations also show a significant deterioration of the model's performance when using the n-factor method (i.e. MC2 and MC3) to estimate ground surface temperature. In both MC2 and MC3, ground thaw rates are significantly underestimated, producing an ALT about 10 to 15 cm below that of the control run at Rio Roca, which already showed an underestimation of the mean ground thaw conditions. At Windy Pass, ALT difference between MC2 and MC3 with the control run is even larger, and between 35 and 40 cm in 2015, and between 43 and 50 cm in 2016. This analysis showed that re-calibrating the n-factor is needed to better simulate ground thaw at these two sites. It is also interesting to note the difference between the MC1 (degree-day) and the control run, as there are two key differences introduced by misrepresenting snow accumulation and melt, the first is the snowcover depletion date, which controls the initiation of ground thaw, and the second is the amount of water that infiltrates the soil which has a significant impact on the thermal conductivity, with wetter thawed soils having a larger thermal conductivity, and thus, higher thawing rates.

Differences in representing ground surface temperature are presented in Table 2. At both sites, the MC1 and MC3 showed the worst

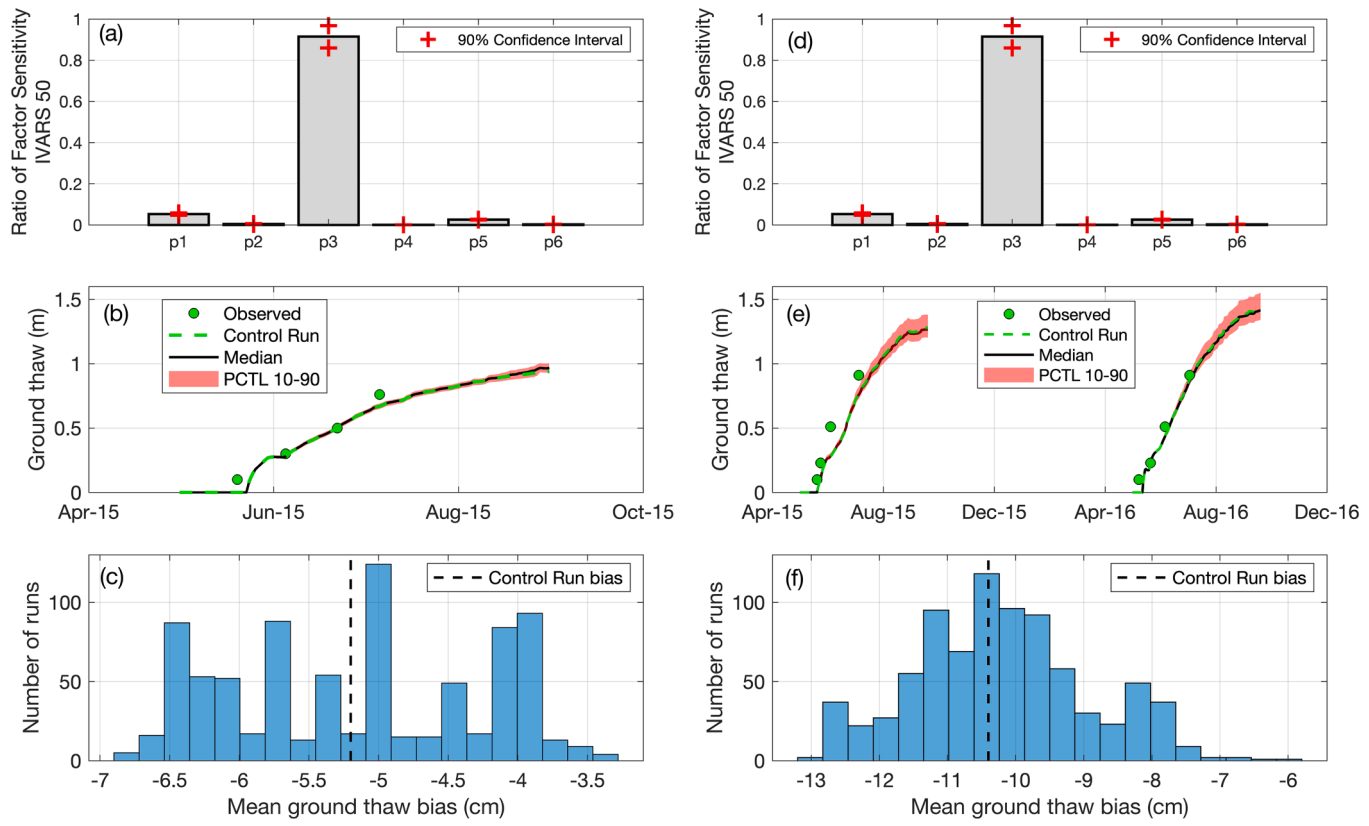

Fig. 7. Results from sensitivity analysis using VARS at Rio Roca (left) and Windy Pass (right). (a) and (d) Ratio of factor sensitivity of simulated ground thaw to selected parameters at Windy Pass; p1: organic layer porosity, p2: mineral soil layer porosity, p3: organic soil layer dry thermal conductivity, p4: mineral soil layer dry thermal conductivity, p5: organic soil layer unfrozen saturated thermal conductivity, p6: mineral soil layer unfrozen saturated thermal conductivity. (b) and (e) Sensitivity of simulated ground thaw to selected parameters against observations. PCTL 10–90 corresponds to the range between percentiles 10th and 90th of the ensemble runs. (c) and (f) Histogram of simulations mean bias calculated as the mean absolute difference between the simulated and observed ground thaw at four soil depths, as shown in Fig. 6.

performance in both correlations and mean bias, when compared with observed ground surface temperature. Note that using a more physically based approach to simulate both ground surface temperature and ground thaw is not enough to properly represent ground surface temperature, as the impact of misrepresenting snow accumulation and melt (i.e. MC1, degree-day) on ground thaw is also significant, due to its impact on ground thaw initiation and rates. Interestingly, MC2 (i.e. n-factor) has a high correlation, even higher than that of the control run at Rio Roca; however, its mean bias is the largest of all scenarios at 2.35 and 3.75 °C in Rio Roca and Windy Pass, respectively. This suggests that the regionally calibrated n-factor is not suitable to representing ground surface temperature locally.

4.4. Climate warming analysis

Average changes to peak SWE for the two winter seasons at Rio Roca are −31, −40 and −56 mm for the + 2, +4 and + 6 °C scenario, respectively (Fig. 9). At Windy Pass, average changes are −4, −21 and −45 mm, for the + 2, +4 and + 6 °C, respectively, with significant interannual variability. During warmer winters like the 2015–2016, the snowpack is more sensitive to increases in temperature producing mid-winter melt events, as shown for Windy Pass (warmer snowpack), or precipitation phase may shift from snowfall to rainfall, reducing snow accumulation. This is particularly important at the beginning and end of the accumulation season and can provide extra energy to melt the snowpack (Pomeroy et al., 2016). Not only peak SWE changed considerably after warming, advances in the date of peak SWE and the end of snow depletion were also found (Table A5). For example, the date of peak SWE at Rio Roca for the 2014–2015 winter shifted earlier by about two to three weeks, whereas it changed little for the 2015–2016 winter. Changes to the snowpack not only impact the amount of water available for spring and summer runoff, but also change the date of the ground thaw initiation, as discussed in previous sections.

Significant changes to ground thaw were found under the warming scenarios. For the + 2 °C scenario at Rio Roca, ALT increased 17 cm or 18%, whereas for the + 6 °C scenario it increased up to 50 cm or 53%. Ground thaw initiation advanced between one to three weeks as temperatures increase at Rio Roca, increasing the duration of the thawing seasons for about one to two months for the + 2 and + 6 °C scenarios, respectively (Table A4). More severe changes to ALT were found at the Windy Pass site (Table A5), particularly during the 2015 summer, with a 26 cm or 20% increase in the + 2 °C scenario, and a 61 cm or 48% increase in the + 6 °C scenario. Changes to the end of the ground thaw season at Windy Pass are not as severe as those found at Rio Roca, with the only significant changes found for the + 4 and + 6 °C scenarios, by about a week during the 2016 summer. The duration of the thawing season at Windy Pass increased by 40 and 25 days for the 2015 and 2016 summer, and the + 6 °C scenario. Overall, results associated to changes to ground thaw showed that ALT at Windy Pass is more sensitive to increasing temperature, which is likely due to the generally longer thawing season than at Rio Roca. However, the initiation, end and duration of the thawing season are more sensitive at the Rio Roca site.

5. Discussion

The site-scale application of the CRHM-AHM model successfully

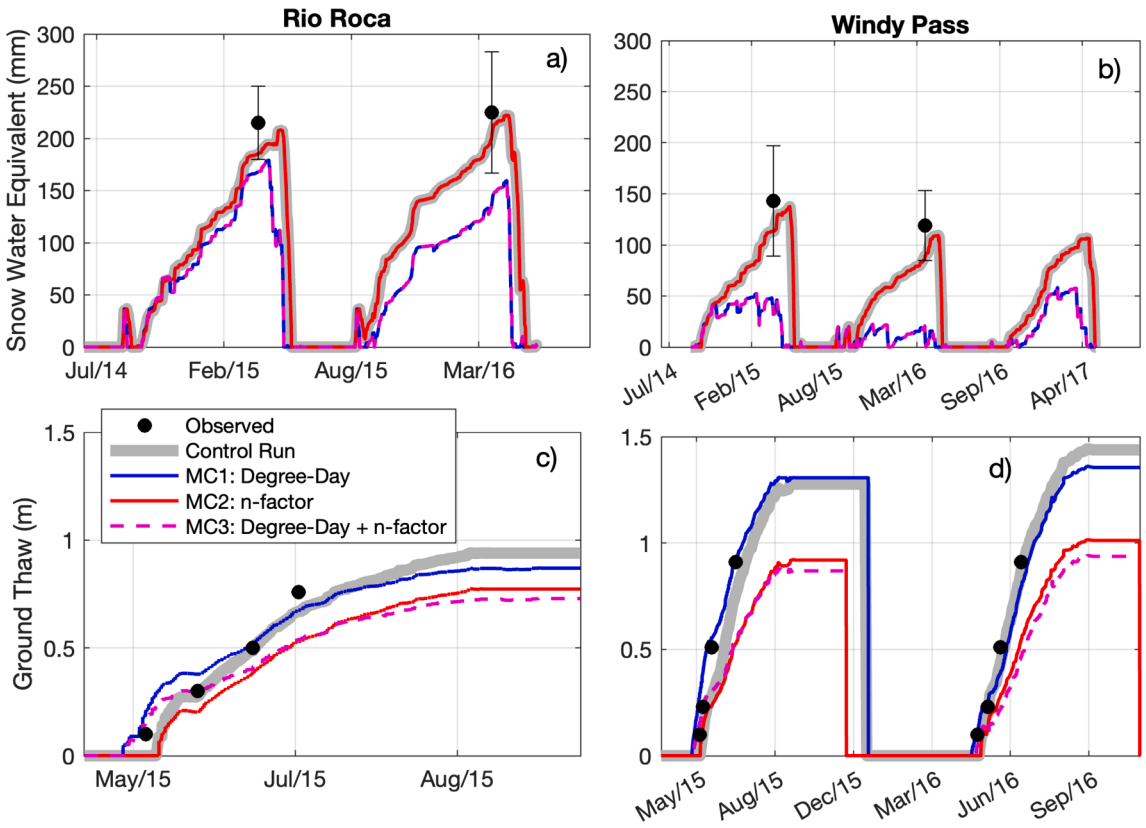

Fig. 8. Model configuration analysis at Rio Roca showing snow water equivalent (a) and ground thaw (c), and at Windy Pass for snow water equivalent (b) and ground thaw (d). Mean snow survey and standar deviation is shown by the black circles with the error bar in (a) and (b).

represented daily ground surface temperature at the two sites (Fig. 5), demonstrating the capacity of the RCC model to be successfully transferred and applied to different conditions without calibration. Ground surface temperature is a critical state variable in the model, as it is used as the upper boundary condition to the module simulating ground thaw, and it is typically used for that purpose by other models as well (Hayashi et al., 2007; Kurylyk et al., 2014; Woo et al., 2007). The model slightly underestimated ground thaw at both sites (Fig. 6). Model underestimation of ground thaw could be due to late simulations of the initiation of ground thaw, which is controlled partially by the end of the snow ablation and meteorological inputs. Simulated end of snow ablation at Windy Pass was three days earlier in 2015 and six days later in 2016; therefore, the later snow disappearance in 2016 can partially explain for the underestimation of ground thaw during 2016 but not during the 2015 thawing season. Differences between simulated and observed snow depth at Windy Pass may be due to several factors including the lack of representation of blowing snow redistribution over complex terrain by the site-scale CRHM-AHM model. As the model implementation uses a single hydrological response unit, it neglects any spatial heterogeneity in the terrain that may also explain for differences in the snowpack and ground thaw between simulations and observations. Unfortunately, measured snow depth at Rio Roca was too noisy to extract a reasonable estimation for the end of the snow ablation. Another reason to explain the underestimation of ground thaw is an underestimation of the saturated thermal conductivity which in combination with the degree of saturation of the soil define the unsaturated thermal conductivity. This application of the CRHM-AHM model does not represent inputs of lateral subsurface flow but it allows outflows, which may impact the accurate representation of the subsurface water storage. In either case, the average underestimation of ground thaw is considered small for hydrological applications, particularly, when parameters from the literature are being used as opposed to measured or locally calibrated values. This is an important finding, as hydrological models of headwater basins in the Arctic typically either neglected or used simplified representations of ground thaw (i.e. degree-day; Zhang et al., 2000; Schramm et al., 2007); however, the CRHM-AHM successfully represented the evolution of the active layer using a robust yet computationally inexpensive approach.

Table 2
Snow-free ground surface temperature performance.

Performance		MC1	MC2	MC3	Control Run
Rio Roca	Correlation	0.55	0.90	0.55	0.88
	Mean Bias (°C)	1.27	2.35	3.11	0.05
Windy Pass	Correlation	0.72	0.90	0.75	0.94
	Mean Bias (°C)	0.62	3.75	4.29	0.01

The sensitivity analysis showed that the parameters associated with the upper organic soil layer are the most important in the model's behaviour (Fig. 7a and 7d); however, this is not particularly surprising, as this layer has the lowest thermal conductivity. Nevertheless, finding this expected behaviour is reassuring of a reasonable process representation by the model. This analysis also showed that mean differences between observed soil temperature and simulations (Fig. 7b and 7e) are not very sensitive to parameter selection, with the largest uncertainty in the relatively warmer and deeper active layer found at the Windy Pass site (Fig. 5). Therefore, although there is uncertainty in parameter selection, it was shown that it does not significantly impact ground thaw simulations, demonstrating the robustness of the model when using a realistic set of physical parameters.

This study investigated the effect of different modelling decisions associated with changing the complexity of some parameterizations on the model's performance. The two-layer energy and mass balance model

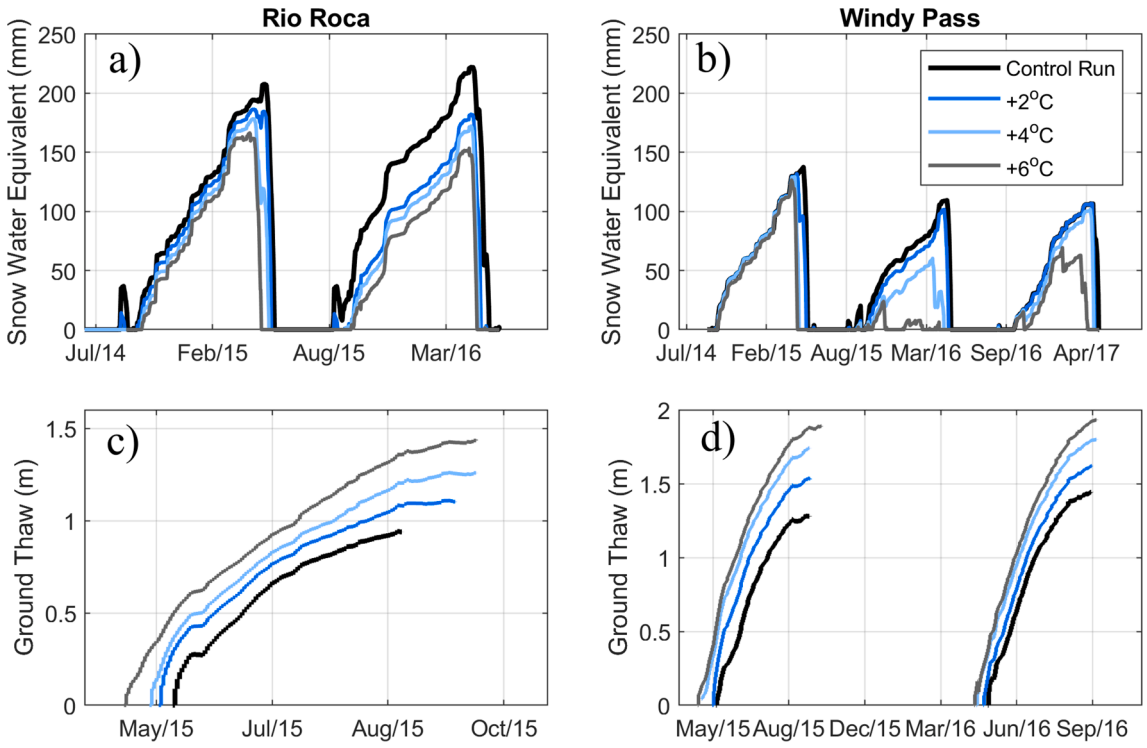

Fig. 9. Projected changes to snow water equivalent at Rio Roca (a) and Windy Pass (b), and ground thaw projections at Rio Roca (c) and Windy Pass (d) under three warming scenarios (+2, +4 and +6 °C).

SNOBAL (Marks et al., 1998) was replaced with a degree-day approach that has been used in previous Arctic hydrological studies (Hinzman and Kane, 1992; Kane et al., 1997) and persists in many hydrological models, though more recent modelling applications in the Arctic have moved toward energy balance type of models (e.g. Krogh et al., 2017; Zhang et al., 2000). Also, the representation of ground surface temperature by the RCC approach (Williams et al., 2015) was replaced by the empirical n-factor (Woo et al., 2007). This analysis revealed the importance of pursuing more physically based approaches to represent Arctic subsurface hydrology as this showed a significantly improved performance without calibration. However, if no other alternative is feasible, empirical approaches like the n-factor may still provide reasonable estimates when their parameters are well calibrated or constrained. Using non-calibrated empirically based approaches significantly deteriorated the performance of the hydrological model. SWE was largely underestimated at both study sites and during each water year, impacting the representation of other processes, such as ground thaw (Fig. 8). The impact of changing the representation of ground surface temperature had a significant effect on ground thaw, reducing the ALT by 10 and 15 cm at Rio Roca, and by 35 to 40 cm at Windy Pass. Such changes in the representation of the ALT can have significant runoff and subsurface storage effects at the hillslope to basin scale (Woo, 2012). This also influences the depth of the subsurface water table, which in turn impact the effective subsurface hydraulic conductivity, subsurface flow and connectivity (Connon et al., 2014; Quinton and Carey, 2008; Quinton and Gray, 2003).

This study examined three scenarios of increasing mean air temperature by + 2, +4 and + 6 °C, which are expected to represent conservative, significant, and severe warming projections. Warming projections by the end of the century for the Canadian Arctic under the RCP8.5 scenario (Riahi et al., 2011) by Li et al. (2019) show that northwestern Canada is projected to warm up to 10 °C in the winter and up to 4 °C in the summer. Air temperature projections from Li et al. (2019) for the region encompassing the Rio Roca and Windy Pass sites, are not as severe as others in northwestern Canada but are still very significant, with increases in winter air temperature of about 5–6 °C (within the range of the sensitivity analysis). The impact of the three warming scenarios on the snowpack at Rio Roca and Windy Pass showed decreasing peak snow accumulation, shortening of the snowcovered season, and earlier date of the snow depletion, with great interannual variability (Fig. 9). These changes are explained by shifting snowfall to rainfall and a warmer snowpack more susceptible to melt, which other studies have shown for other sites in the region (Krogh and Pomeroy, 2019; Rasouli et al., 2019). Changes to the ALT go from roughly 17 cm or 18% at Rio Roca, up 61 cm or 48% at Windy Pass, for the moderate (+2°C) and severe (+6°C) warming scenarios, respectively. Changes to the duration of the ground thaw season also showed a significant increase up to one to two months for the severe (+6°C) warming scenario, whereas for the moderate scenario (+2°C) it increased between one to four weeks, with the colder Rio Roca site showing the largest changes. Changes to the ALT under changing climate scenarios have been previously studied for other sites in the region. Park et al. (2015) studied the impact that changing precipitation, and thus the snowpack extent and depth, at the pan-Arctic scale using a process-based land surface model. They found that the ALT was the most sensitive to changes in Autumn snowpack conditions, with larger early-season snowpacks having the deeper next-season ALT due to the isolation effect of the snowpack to the cold winter temperatures. Similarly to Park et al. (2015), we show that the snowpack has a significant impact on the development of the ALT; however, we relate it to the peak snow accumulation. We found that

shallower end-of-the-winter snowpacks that fully ablate earlier in the season allow for an earlier initiation of ground thaw, and thus deeper ALTs (Fig. 9). This highlights the importance of accurately simulating snowpack processes to properly capture permafrost dynamics. Woo et al. (2007) investigated changes to the ALT at several sites with different soil cover and two climate scenarios (A2 and B2), and found that for the most severe scenario (A2), increases to the ALT were around 30 cm by the end of the century for the sites covered by a thin layer of peat (20 cm) and about 10 cm thicker for the sites with a thick 1-m peat cover, both within the range of expected sensitivity presented in this study (Fig. 9). Krogh and Pomeroy (2019) used the CRHM-AHM and climate projections by Li et al. (2019) (about 6 °C increase in mean annual air temperature), at a basin near Inuvik, NWT. They found average increases to ALT of 25 cm and a thawing season extended by about three weeks by the end of the century, which are within the range of changes found in this study. Results from the air temperature sensitivity analysis are likely to be representative of other relatively flat Arctic basins with a similar soil layer configuration; however, they might vary significantly in steeper places or places with deeper snowpacks.

6. Conclusions

This study demonstrated that a robust and yet computationally inexpensive algorithm to represent active layer development in regions underlain by continuous permafrost can be successfully coupled to a physically based hydrological model for cold regions providing reasonable estimates at two relatively level tundra sites in northwestern Canada. Although differences in simulating the end of the snow ablation (up to six days) and the active layer development (up to 15 cm) were found, these are considered reasonable for hydrological applications supporting the transferability of them model to other Arctic regions. The sensitivity analysis of key soil thermal properties and porosity demonstrated the robust representation of ground thaw, where results did not significantly change when using a realistic range for the physical parameters, supporting the model's implementation in places with little soil information. The modelling decision analysis revealed that implementing non-calibrated, empirically based algorithms using available regional information to represent snowpack dynamics and ground surface temperature resulted in a significant deterioration of the model's performance. This supports the fact that the Arctic and, more generally, cold regions hydrology would benefit from more physically based algorithms to produce more realistic hydrological simulations (at least at the scale of the presented analysis). This appears to be particularly true in remote, poorly monitored regions, where empirically based algorithms are more prone to failure due to lack of data for calibration and incomplete coupling of mass and energy budgets. The air temperature sensitivity analysis showed substantial increases in active layer thickness, declining snow accumulation and earlier snowmelt with increasing air temperature, which can help informing policy makers in the region as climate change progresses.

Author contributions

SK and JP designed the study and helped in the installation of the monitoring stations. SK performed the simulations and analyzed the results. SK wrote the first draft of the manuscript which was then reviewed and discussed with JP.

Declaration of Competing Interest

The authors declare that they have no known competing financial interests or personal relationships that could have appeared to influence the work reported in this paper.

Acknowledgments

The authors thank the late Ric Janowicz (Yukon Environment), Sean Carey (McMaster University) and Tyler Williams (Yukon Environment) for their support in the installation, maintenance, and collection of data at the research sites. Funding for this study was provided by Yukon Environment, NSERC Discovery Grants, NSERC Changing Cold Regions Network, the CFREF-funded Global Water Futures program, the CRC program and CONICYT under the PhD Becas Chile scholarship program. This paper is dedicated to the memory of Ric Janowicz, Senior Hydrologist for Yukon Environment who led the development of Northern Hydrology in Yukon and was a key contributor to the development of the Cold Regions Hydrological Model. We thank the two anonymous reviewers for their helpful comments.

Appendix A

Table A1
Recorded soil temperature profile for the period spring 2015 – spring 2016 at Rio Roca.

Depth (cm)	Ground thaw initiation	Ground freeze initiation	Thaw season duration (days)	Maximum Temperature (°C)	Minimum Temperature (°C)
10	May 20	Oct 2	135	9.0	−4.6
30	June 1	Oct 9	130	5.5	−3.5
50	June 22	Oct 9	109	4.2	−2.7
76	July 5	Oct 15	102	2.2	−2.1

Table A2
Recorded soil temperature for the period spring 2015 – spring 2017 at Windy Pass.

	Depth (cm)	Ground thaw initiation	Ground freeze initiation	Thaw season duration (days)	Maximum 6-hourly temperature (°C)	Minimum 6-hourly temperature (°C)
Spring 2015 – Spring 2016	10	May 19	Oct 11	145	13.5	−8.1
	23	May 22	Nov 15	177	9.7	−4.6
	51	May 31	Dec 25	208	7.8	−1.6
	91	June 30	Feb 9	255	6.5	−0.5
Spring 2016 – Spring 2017	10	April 30	Oct 9	162	16.4	−3.9
	23	May 19	Nov 4	152	12.1	−1.9
	51	June 5	Jan 15	224	9.3	−0.7
	91	July 2	Apr 23	295	8.1	−0.1

Table A3
Description of the physical processes included in the hydrological model for Rio Roca and Windy Pass.

Physical process	Module description
Precipitation Phase Partition	This method estimates the phase of precipitation (rain or snow) using a psychrometric energy balance approach, based on the fall velocity, air temperature and the relative humidity (Harder and Pomeroy, 2013).
Albedo Decay	Albedo decay rate is classified into three groups: premelt, melt and postmelt, each with a different decay rate for the snowcovered period. This model is suitable for cold shallow snowpacks that are not subject to frequent mid-winter melt events (Gray and Landine, 1987).
Canopy Interception, Sublimation and Evaporation	The Rutter Interception Model (Valente et al., 1997) for rain interception, linked to growing season evapotranspiration. The Canopy Interception and Sublimation Model for the snow season (Ellis et al., 2010; Hedstrom and Pomeroy, 1998; Parviainen and Pomeroy, 2000; Pomeroy et al., 1998).
Snow Melt and Accumulation	A Snowcover Energy Balance Model (SNOBAL; Marks et al., 1998) is a two-layer energy balance model that allows refreezing and uses the bulk transfer method with stability correction (Monin and Obukhov, 1954) to calculate turbulent heat fluxes.
Evapotranspiration	Penman-Monteith Algorithm (P-M; Monteith, 2007) for unsaturated surfaces and Priestley-Taylor (Priestley and Taylor, 1972) for saturated surfaces. Jarvis (1976) to estimate stomata resistance changes.
Blowing Snow Transport, Sublimation and Redistribution	Prairie Blowing Snow Model (PBSM; Fang and Pomeroy, 2009; Pomeroy and Li, 2000) is a steady-state two-phase flow model that calculates snow saltation and suspension based on friction velocity, aerodynamic roughness height, exposed vegetation, and fetch distance. A coupled sublimation algorithm integrates the sublimation of a single ice particle over the saltation and suspension layers and rescales this to bulk sublimation.
Ground Thaw-Freeze	A simplified solution of Stefan's heat flow equation, the XG – algorithm (Changwei and Gough, 2013).
Snow-free ground surface temperature	Semi-empirical approach that uses air temperature, net radiation, and antecedent frost table depth to estimate ground surface temperature (Williams et al., 2015).
Water flow through snowpack and organic layer	Water flow detention produced by the celerity of flow through the snowpack or exposed organic layers above soil is calculated as per Pomeroy et al. (2016) based on Colbeck (1975) and Colbeck (1972) and relationships between permeability, water pressure and saturation.
Soil Infiltration	Infiltration into unfrozen soils using (Ayers, 1959) and into frozen soils using Gray et al. (2001). Infiltration into unfrozen soils is based on an empirical relationship between ground cover condition (e.g., bare soil or forested) and soil texture. For frozen soils, infiltration is first classified as unlimited, restricted and limited. For limited infiltration, parameterization of a finite difference heat and mass transfer model is based on initial surface saturation, average soil saturation and temperature, and infiltration opportunity time.
Soil Moisture	Subsurface vertical and lateral drainage controlled by effective hydraulic conductivity using the Brooks & Corey (1964) relationship. Three-layer model includes a recharge, lower and groundwater layer. The model allows for infiltration excess or saturation-excess overland flow, surface runoff, recharge through macropores and subsurface discharge (Fang et al., 2012). Here, no sub-permafrost groundwater recharge is allowed due to ice-rich soils and relatively shallow active layer. Lateral and vertical flows are calculated based on Darcy's law using the unsaturated hydraulic conductivity calculated with the Brooks and Corey (1964) relationship. This module is linked to XG and all water and storage capacity in the frozen layer is considered immobile and inaccessible. Liquid water below a frozen layer may drain vertically or horizontally but not be recharged from above. Liquid water above a frozen layer is restricted to the unfrozen layer and may drain horizontally and be recharged or withdrawn by evapotranspiration.
Surface and Subsurface Routing	Surface and subsurface lag and storage (Clark, 1945).

Table A4
Changes to key SWE and ground thaw characteristics for the Control Run and the climate warming scenarios at Rio Roca. CR: Control Run.

	Rio Roca (2015)				Rio Roca (2016)			
Temperature increase	CR	+2 °C	+4 °C	+6 °C	CR	+2 °C	+4 °C	+6 °C
Snow Disappearance Date	21-May	16-May	12-May	29-Apr	23-May	9-May	6-May	2-May
Date of Peak SWE	5-May	14-Apr	14-Apr	9-Apr	22-Apr	22-Apr	22-Apr	19-Apr
Peak SWE (mm)	208	186	178	166	222	182	172	153
Ground thaw initiation	23-May	17-May	13-May	2-May	n/a	n/a	n/a	n/a
Ground thaw end	30-Aug	22-Sep	1-Oct	1-Oct	n/a	n/a	n/a	n/a
Ground thaw duration (days)	99	128	141	152	n/a	n/a	n/a	n/a
Active Layer Thickness (m)	0.94	1.11	1.26	1.44	n/a	n/a	n/a	n/a
Mean ground thaw rate (cm/d)	0.95	0.87	0.89	0.95	n/a	n/a	n/a	n/a

Table A5
Changes to key SWE and ground thaw characteristics for the Control Run and the climate warming scenarios at Windy Pass. CR: Control Run.

	Windy Pass (2015)				Windy Pass (2016)				Windy Pass (2017)			
Temperature increase	CR	+2 °C	+4 °C	+6 °C	CR	+2 °C	+4 °C	+6 °C	CR	+2 °C	+4 °C	+6 °C
Snow Disappearance Date	19-May	15-May	27-Apr	23-Apr	11-May	5-May	23-Apr	11-Apr	15-May	5-May	3-May	18-Apr
Date of Peak SWE	8-May	22-Apr	16-Apr	8-Apr	1-May	24-Apr	26-Mar	24-Feb	25-Apr	26-Apr	24-Apr	14-Feb
Peak SWE (mm)	137	132	129	127	109	102	60	8	107	107	102	69
Ground thaw initiation	20-May	15-May	1-May	26-Apr	12-May	6-May	27-Apr	24-Apr	n/a	n/a	n/a	n/a
Ground thaw end	20-Sep	21-Sep	20-Sep	6-Oct	25-Sep	26-Sep	2-Oct	2-Oct	n/a	n/a	n/a	n/a
Ground thaw duration (days)	123	129	142	163	136	143	158	161	n/a	n/a	n/a	n/a
Active Layer Thickness (m)	1.28	1.54	1.74	1.89	1.44	1.62	1.80	1.93	n/a	n/a	n/a	n/a
Mean ground thaw rate (cm/d)	1.04	1.19	1.23	1.16	1.06	1.13	1.14	1.20	n/a	n/a	n/a	n/a

References

Atchley, A.L., Painter, S.L., Harp, D.R., Coon, E.T., Wilson, C.J., Liljedahl, A.K., Romanovsky, V.E., 2015. Using field observations to inform thermal hydrology models of permafrost dynamics with ATS (v0.83). Geosci. Model Dev. 8, 2701–2722. https://doi.org/10.5194/gmd-8-2701-2015.

Brown, J., Ferrians, J.O., Heginbottom, J.A., Melnikov, A., 2002. Circum-Arctic Map of Permafrost and Ground-Ice Contitions, Verions 2. https://doi.org/10.7265/skbg-kf16.

Connon, R.F., Quinton, W.L., Craig, J.R., Hayashi, M., 2014. Changing hydrologic connectivity due to permafrost thaw in the lower Liard River valley, NWT, Canada. Hydrol. Process. 28, 4163–4178. https://doi.org/10.1002/hyp.10206.

Endrizzi, S., Gruber, S., Dall'Amico, M., Rigon, R., 2014. GEOtop 2.0: simulating the combined energy and water balance at and below the land surface accounting for soil freezing, snow cover and terrain effects. Geosci. Model Dev. 7 (6), 2831–2857. https://doi.org/10.5194/gmd-7-2831-201410.5194/gmd-7-2831-2014-supplement.

Fox, J.D., 1992. Incorporating freeze-thaw calculations into a water balance model. Water Resour. Res. 28 (9), 2229–2244. https://doi.org/10.1029/92WR00983.

Goodison, B.E., Louie, P.Y., Yang, D., 1998. WMO Solid Precipitation Measurement Intercomparison. Report No. 67, World Meteorological Organization.

Hayashi, M., Goeller, N., Quinton, W.L., Wright, N., 2007. A simple heat-conduction method for simulating the frost-table depth in hydrological models. Hydrol. Process. 21 (19), 2610–2622. https://doi.org/10.1002/(ISSN)1099-108510.1002/hyp.v21:1910.1002/hyp.6792.

Herndon, E.M., 2018. Permafrost slowly exhales methane. Nat. Clim. Chang. 8 (4), 273–274. https://doi.org/10.1038/s41558-018-0129-6.

Hinzman, L.D., Kane, D.L., 1992. Potential Response of an Arctic Watershed During a Period of Global Warming. J. Geophys. Res. 97, 2811–2820. https://doi.org/10.1029/91JD01752.

Jan, A., Coon, E.T., Painter, S.L., 2020. Evaluating integrated surface/subsurface permafrost thermal hydrology models in ATS (v0.88) against observations from a polygonal tundra site. Geosci. Model Dev. 13 (5), 2259–2276. https://doi.org/10.5194/gmd-13-2259-202010.5194/gmd-13-2259-2020-supplement.

Jan, A., Coon, E.T., Painter, S.L., Garimella, R., Moulton, J.D., 2018. An intermediate-scale model for thermal hydrology in low-relief permafrost-affected landscapes. Comput. Geosci. 22 (1), 163–177. https://doi.org/10.1007/s10596-017-9679-3.

Johansen, O., 1975. Thermal Conductitivy of Soils. CRREL Draft Translation 637, 1977, ADA 044002, 291p. Johansson.

Juminikis, A.R., 1977. Thermal Geotechnics. Rutgers University Press, New Brunswick, New Jersey.

Kane, D.L., Gieck, R.E., Hinzman, L.D., 1997. Snowmelt Modeling at Small Alaskan Arctic Watershed. J. Hydrol. Eng. 2 (4), 204–210. https://doi.org/10.1061/(ASCE)1084-0699(1997)2:4(204).

Kane, D.L., Hinzman, L.D., Benson, C.S., Liston, G.E., 1991. Snow hydrology of a headwater arctic basin, 1. Physical measurements and process studies. Water Resour. Res. 27 (6), 1099–1109. https://doi.org/10.1029/91WR00262.

Klene, A.E., Nelson, F.E., Shiklomanov, N.I., Hinkel, K.M., 2001. The N-Factor in Natural Landscapes: Variability of Air and Soil-Surface Temperatures, Kuparuk River Basin, Alaska, U.S.A. Arctic, Antarct. Alp. Res. 33, 140. https://doi.org/10.2307/1552214.

Knoblauch, C., Beer, C., Liebner, S., Grigoriev, M.N., Pfeiffer, E.-M., 2018. Methane production as key to the greenhouse gas budget of thawing permafrost. Nat. Clim. Chang. 8 (4), 309–312. https://doi.org/10.1038/s41558-018-0095-z.

Krogh, S.A., Pomeroy, J.W., 2019. Impact of Future Climate and Vegetation on the Hydrology of an Arctic Headwater Basin at the Tundra-Taiga Transition. J. Hydrometeorol. 20, 197–215. https://doi.org/10.1175/JHM-D-18-0187.1.

Krogh, S.A., Pomeroy, J.W., 2018. Recent changes to the hydrological cycle of an Arctic basin at the tundra–taiga transition. Hydrol. Earth Syst. Sci. 22, 3993–4014. https://doi.org/10.5194/hess-22-3993-2018.

Krogh, S.A., Pomeroy, J.W., Marsh, P., 2017. Diagnosis of the hydrology of a small Arctic basin at the tundra-taiga transition using a physically based hydrological model. J. Hydrol. 550, 685–703. https://doi.org/10.1016/j.jhydrol.2017.05.042.

Kurylyk, B.L., McKenzie, J.M., MacQuarrie, K.T.B., Voss, C.I., 2014. Analytical solutions for benchmarking cold regions subsurface water flow and energy transport models: One-dimensional soil thaw with conduction and advection. Adv. Water Resour. 70, 172–184. https://doi.org/10.1016/j.advwatres.2014.05.005.

Kurylyk, B.L., Watanabe, K., 2013. The mathematical representation of freezing and thawing processes in variably-saturated, non-deformable soils. Adv. Water Resour. 60, 160–177. https://doi.org/10.1016/j.advwatres.2013.07.016.

Kustas, W.P., Rango, A., Uijlenhoet, R., 1994. A simple energy budget algorithm for the snowmelt runoff model. Water Resour. Res. 30 (5), 1515–1527. https://doi.org/10.1029/94WR00152.

Lantz, T.C., Marsh, P., Kokelj, S.V., 2013. Recent Shrub Proliferation in the Mackenzie Delta Uplands and Microclimatic Implications. Ecosystems 16 (1), 47–59. https://doi.org/10.1007/s10021-012-9595-2.

Li, Y., Li, Z., Zhang, Z., Chen, L., Kurkute, S., Scaff, L., Pan, X., 2019. High-Resolution Regional Climate Modeling and Projection over Western Canada using a Weather Research Forecasting Model with a Pseudo-Global Warming Approach. Hydrol. Earth Syst. Sci. Discuss. 1–38 https://doi.org/10.5194/hess-2019-201.

Liljedahl, A.K., Boike, J., Daanen, R.P., Fedorov, A.N., Frost, G.V., Grosse, G., Hinzman, L.D., Iijma, Y., Jorgenson, J.C., Matveyeva, N., Necsoiu, M., Raynolds, M. K., Romanovsky, V.E., Schulla, J., Tape, K.D., Walker, D.A., Wilson, C.J., Yabuki, H., Zona, D., 2016. Pan-Arctic ice-wedge degradation in warming permafrost and its influence on tundra hydrology. Nat. Geosci. 9 (4), 312–318. https://doi.org/10.1038/ngeo2674.

Marks, D., Kimball, J., Tingey, D., Link, T., 1998. The sensitivity of snowmelt processes to climate conditions and forest cover during rain-on-snow: a case study of the 1996 Pacific Northwest flood. Hydrol. Process. 12, 1569–1587. https://doi.org/10.1002/(SICI)1099-1085(199808/09)12:10/11<1569::AID-HYP682>3.0.CO;2-L.

McKenzie, J.M., Voss, C.I., Siegel, D.I., 2007. Groundwater flow with energy transport and water-ice phase change: Numerical simulations, benchmarks, and application to freezing in peat bogs. Adv. Water Resour. 30 (4), 966–983. https://doi.org/10.1016/j.advwatres.2006.08.008.

Myers-Smith, I.H., Harden, J.W., Wilmking, M., Fuller, C.C., McGuire, A.D., Chapin, F.S., 2008. Wetland succession in a permafrost collapse: interactions between fire and thermokarst. Biogeosciences 5 (5), 1273–1286. https://doi.org/10.5194/bg-5-1273-2008.

Myers-Smith, I.H., Hik, D.S., Aerts, R., 2018. Climate warming as a driver of tundra shrubline advance. J. Ecol. 106 (2), 547–560. https://doi.org/10.1111/1365-2745.12817.

Painter, S.L., Coon, E.T., Atchley, A.L., Berndt, M., Garimella, R., Moulton, J.D., Svyatskiy, D., Wilson, C.J., 2016. Integrated surface/subsurface permafrost thermal hydrology: Model formulation and proof-of-concept simulations. Water Resour. Res. 52 (8), 6062–6077. https://doi.org/10.1002/2015WR018427.

Park, H., Fedorov, A.N., Zheleznyak, M.N., Konstantinov, P.Y., Walsh, J.E., 2015. Effect of snow cover on pan-Arctic permafrost thermal regimes. Clim. Dyn. 44 (9-10), 2873–2895. https://doi.org/10.1007/s00382-014-2356-5.

Payette, S., 2004. Accelerated thawing of subarctic peatland permafrost over the last 50 years. Geophys. Res. Lett. 31, L18208. https://doi.org/10.1029/2004GL020358.

Pomeroy, J.W., Fang, X., Marks, D.G., 2016. The Cold Rain-on-Snoe Event of June 2013 in the Canadian Rockies - Characteristics and Diagnosis. Hydrol. Process. 30, 2899–2914. https://doi.org/10.1002/hyp.10905.

Pomeroy, J.W., Gray, D.M., Brown, T., Hedstrom, N.R., Quinton, W.L., Granger, R.J., Carey, S.K., 2007. The cold regions hydrological model: a platform for basing process representation and model structure on physical evidence. Hydrological 21, 1–27. https://doi.org/10.1002/hyp.

Pomeroy, J.W., Spence, C., Whitfield, P.H., Spence, C., 2013. Putting Prediction in Ungauged Basins into Practice. Canadian Water Resources Association.

Quinton, W.L., Carey, S.K., 2008. Towards an energy-based runoff generation theory for tundra landscapes. Hydrol. Process. 22 (23), 4649–4653. https://doi.org/10.1002/hyp.v22:2310.1002/hyp.7164.

Quinton, W.L., Gray, D.M., 2003. Subsurface drainage from organic soils in permafrost terrain : the major factors to be represented in a runoff model, in: Proceedings of the Eighth International Conference on Permafrost. Davos, Switzerland, p. 6.

Rasouli, K., Pomeroy, J.W., Whitfield, P.H., 2019. Hydrological Responses of Headwater Basins to Monthly Perturbed Climate in the North American Cordillera. J. Hydrometeorol. 20, 863–882. https://doi.org/10.1175/JHM-D-18-0166.1.

Razavi, S., Gupta, H.V., 2016. A new framework for comprehensive, robust, and efficient global sensitivity analysis: 2. Application. Water Resour. Res. 52 (1), 440–455. https://doi.org/10.1002/wrcr.v52.110.1002/2015WR017559.

Razavi, S., Sheikholeslami, R., Gupta, H.V., Haghnegahdar, A., 2019. VARS-TOOL: A toolbox for comprehensive, efficient, and robust sensitivity and uncertainty analysis. Environ. Model. Softw. 112, 95–107. https://doi.org/10.1016/j.envsoft.2018.10.005.

Riahi, K., Rao, S., Krey, V., Cho, C., Chirkov, V., Fischer, G., Kindermann, G., Nakicenovic, N., Rafaj, P., 2011. RCP 8.5—A scenario of comparatively high greenhouse gas emissions. Clim. Change 109 (1-2), 33–57. https://doi.org/10.1007/s10584-011-0149-y.

Schramm, I., Boike, J., Bolton, W.R., Hinzman, L.D., 2007. Application of TopoFlow, a spatially distributed hydrological model, to the Imnavait Creek watershed. Alaska. J. Geophys. Res. 112 (G4), n/a–n/a. https://doi.org/10.1029/2006JG000326.

Sicart, J.E., Pomeroy, J.W., Essery, R.L.H., Bewley, D., 2006. Incoming longwave radiation to melting snow: observations, sensitivity and estimation in Northern environments. Hydrol. Process. 20 (17), 3697–3708. https://doi.org/10.1002/(ISSN)1099-108510.1002/hyp.v20:1710.1002/hyp.6383.

Sivapalan, M., 2003. Prediction in ungauged basins: a grand challenge for theoretical hydrology. Hydrol. Process. 17 (15), 3163–3170. https://doi.org/10.1002/(ISSN)1099-108510.1002/hyp.v17:1510.1002/hyp.5155.

Smith, C., 2008. Correcting the wind bias in snowfall measurements made with a Geonor T-200B precipitation gauge and alter wind shield. CMOS Bulletin SCMO 162–167.

Sturm, M., Racine, C., Tape, K., 2001. Increasing shrub abundance in the Arctic. Nature 411 (6837), 546–547. https://doi.org/10.1038/35079180.

Suzuki, K., Matsuo, K., Yamazaki, D., Ichii, K., Iijima, Y., Papa, F., Yanagi, Y., Hiyama, T., 2018. Hydrological Variability and Changes in the Arctic Circumpolar Tundra and the Three Largest Pan-Arctic River Basins from 2002 to 2016. Remote Sens. 10, 402. https://doi.org/10.3390/rs10030402.

Walvoord, M.A., Kurylyk, B.L., 2016. Hydrologic impacts of thawing permafrost - a review. Vadose Zo. J. 15, 1–20. https://doi.org/10.2136/vzj2016.01.0010.

Williams, T.J., Pomeroy, J.W., Janowicz, J.R., Carey, S.K., Rasouli, K., Quinton, W.L., 2015. A radiative-conductive-convective approach to calculate thaw season ground surface temperatures for modelling frost table dynamics. Hydrol. Process. 29, 3954–3965. https://doi.org/10.1002/hyp.10573.

Woo, M.-K., 2012. Permafrost Hydrology. Springer, Berlin Heidelberg, Berlin, Heidelberg. https://doi.org/10.1007/978-3-642-23462-0.

Woo, M.-k., Mollinga, M., Smith, S.L., 2007. Climate warming and active layer thaw in the boreal and tundra environments of the Mackenzie Valley. Can. J. Earth Sci. 44 (6), 733–743. https://doi.org/10.1139/e06-121.

Woo, M.-k., Arain, M.A., Mollinga, M., Yi, S., 2004. A two-directional freeze and thaw algorithm for hydrologic and land surface modelling. Geophys. Res. Lett. 31 (12), 1–4. https://doi.org/10.1029/2004GL019475.

Xie, C., Gough, W.A., 2013. A Simple Thaw-Freeze Algorithm for a Multi-Layered Soil using the Stefan Equation. Permafr. Periglac. Process. 24, 252–260. https://doi.org/10.1002/ppp.1770.

Yamazaki, T., 2001. A One-dimensional Land Surface Model Adaptable to Intensely Cold Regions and its Applications in Eastern Siberia. J. Meteorol. Soc. Japan. Ser. II 79 (6), 1107–1118. https://doi.org/10.2151/jmsj.79.1107.
Yi, S., Arain, M.A., Woo, M.-K., 2006. Modifications of a land surface scheme for improved simulation of ground freeze-thaw in northern environments. Geophys. Res. Lett. 33, L13501. https://doi.org/10.1029/2006GL026340.
Zhang, Z., Kane, D.L., Hinzman, L.D., 2000. Development and application of a spatially-distributed Arctic hydrological and thermal process model (ARHYTHM). Hydrol. Process. 14, 1017–1044. https://doi.org/10.1002/(SICI)1099-1085(20000430)14:6<1017::AID-HYP982>3.0.CO;2-G.
Zhao, L., Gray, D.M., Male, D.H., 1997. Numerical analysis of simultaneous heat and mass transfer during infiltration into frozen ground. J. Hydrol. 200 (1-4), 345–363. https://doi.org/10.1016/S0022-1694(97)00028-0.

Appendix References

Ayers, H.D., 1959. Influence of Soil Profile and Vegetation Characteristic on Net Rainfall Supply to Runoff. In: Spillway Design Floods: Proceeding of Hydrology Symposium No. 1, National Research Council of Canada. pp. 198–205.
Brooks, R., Corey, A., 1964. Hydraulic properties of porous media. Colorado State University, Hydrology Papers.
Changwei, X., Gough, W.A., 2013. A Simple Thaw-Freeze Algorithm for a Multi-Layered Soil using the Stefan Equation. Permafr. Periglac. Process. 24, 252–260. https://doi.org/10.1002/ppp.1770.
Clark, C.O., 1945. Storage and the Unit Hydrograph. Transect. ASCE 110, 1419–1446.
Colbeck, S.C., 1975. A theory for water flow through a layered snowpack. Water Resour. Res. 11, 261–266. https://doi.org/10.1029/WR011i002p00261.
Colbeck, S.C., 1972. A Theory of Water Percolation in Snow. J. Glaciol. 11, 369–385. https://doi.org/10.3189/S0022143000022346.
Ellis, C.R., Pomeroy, J.W., Brown, T., MacDonald, J., 2010. Simulation of snow accumulation and melt in needleleaf forest environments. Hydrol. Earth Syst. Sci. 14, 925–940. https://doi.org/10.5194/hess-14-925-2010.
Fang, X., Pomeroy, J.W., 2009. Modelling blowing snow redistribution to prairie wetlands. Hydrol. Process. https://doi.org/10.1002/hyp.
Fang, X., Pomeroy, J.W., Ellis, C.R., MacDonald, M.K., DeBeer, C.M., Brown, T., 2012. Multi-variable evaluation of hydrological model predictions for a headwater basin in the Canadian Rocky Mountains. Hydrol. Earth Syst. Sci. Discuss. 9, 12825–12877. https://doi.org/10.5194/hessd-9-12825-2012.
Gray, D.M., Landine, P.G., 1987. Albedo model for shallow prairie snow covers. Can. J. Earth Sci. 24, 1760–1768. https://doi.org/10.1139/e87-168.
Gray, D.M., Toth, B., Zhao, L., Pomeroy, J.W., Granger, R.J., 2001. Estimating areal snowmelt infiltration into frozen soils. Hydrol. Process. 15, 3095–3111. https://doi.org/10.1002/hyp.320.
Harder, P., Pomeroy, J.W., 2013. Estimating precipitation phase using a psychrometric energy balance method. Hydrol. Process. 27, 1901–1914. https://doi.org/10.1002/hyp.
Hedstrom, N.R., Pomeroy, J.W., 1998. Measurements and modelling of snow interception in the boreal forest. Hydrol. Process. 12, 1611–1625. https://doi.org/https://doi.org/10.1002/(SICI)1099–1085(199808/09)12:10/11 < 1611::AID-HYP684 > 3.0.CO;2–4.
Jarvis, P.G., 1976. The Interpretation of the Variations in Leaf Water Potential and Stomatal Conductance Found in Canopies in the Field. Philos. Trans. R. Soc. B Biol. Sci. 273, 593–610. https://doi.org/10.1098/rstb.1976.0035.
Monin, A.S., Obukhov, A.M., 1954. Basic laws of turbulent mixing in the surface layer of the atmosphere. In: Proceesings of Geophysiclas Institute. National Academy of Science, SSSR, pp. 163–187.
Monteith, J.L., 2007. Evaporation and surface temperature. Q. J. R. Meteorol. Soc. 107, 1–27. https://doi.org/10.1002/qj.49710745102.
Parviainen, J., Pomeroy, J.W., 2000. Multiple-scale modelling of forest snow sublimation: initial findings. Hydrol. Process. 14, 2669–2681. https://doi.org/10.1002/1099–1085(20001030)14:15<2669::AID-HYP85>3.0.CO;2-Q.
Pomeroy, J.W., Li, L., 2000. Prairie and Arctic areal snow cover mass balance using a blowing snow model. J. Geophys. Res. Atmos. 105, 26619–26634. https://doi.org/10.1029/2000JD900149.
Pomeroy, J.W., Parviainen, J., Hedstrom, N., Gray, D.M., 1998. Coupled modelling of forest snow interception and sublimation. Hydrol. Process. 12, 2317–2337. https://doi.org/10.1002/(SICI)1099-1085(199812)12:15<2317::AID-HYP799>3.0.CO;2-X.
Priestley, C.H.B., Taylor, R.J., 1972. On the Assessment of Surface Heat Flux and Evaporation Using Large-Scale Parameters. Mon. Weather Rev. 100, 81–92. https://doi.org/10.1175/1520-0493(1972)100<0081:OTAOSH>2.3.CO;2.
Valente, F., David, J.S., Gash, J.H.C., 1997. Modelling interception loss for two sparse eucalypt and pine forests in central Portugal using reformulated Rutter and Gash analytical models. J. Hydrol. 190, 141–162. https://doi.org/10.1016/S0022-1694(96)03066-1.